Accepted Manuscript

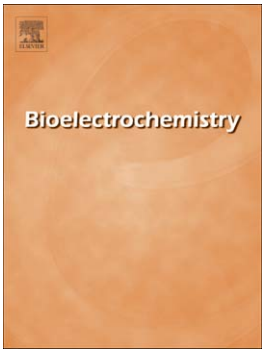

An overview of dealloyed nanoporous gold in bioelectrochemistry

Xinxin Xiao, Pengchao Si, Edmond Magner

PII: S1567-5394(15)30037-2
DOI: doi: 10.1016/j.bioelechem.2015.12.008
Reference: BIOJEC 6903

To appear in: *Bioelectrochemistry*

Received date: 2 November 2015
Revised date: 23 December 2015
Accepted date: 30 December 2015

Please cite this article as: Xinxin Xiao, Pengchao Si, Edmond Magner, An overview of dealloyed nanoporous gold in bioelectrochemistry, *Bioelectrochemistry* (2015), doi: 10.1016/j.bioelechem.2015.12.008

This is a PDF file of an unedited manuscript that has been accepted for publication. As a service to our customers we are providing this early version of the manuscript. The manuscript will undergo copyediting, typesetting, and review of the resulting proof before it is published in its final form. Please note that during the production process errors may be discovered which could affect the content, and all legal disclaimers that apply to the journal pertain.

An overview of dealloyed nanoporous gold in bioelectrochemistry

Xinxin Xiao[a,b], Pengchao Si[*a] and Edmond Magner[*b]

[a]Key Laboratory for Liquid-Solid Structural Evolution and Processing of Materials, Ministry of Education, School of Materials Science and Engineering, Shandong University, Jinan 250061, People's Republic of China. E-mail: pcsi@sdu.edu.cn

[b]Department of Chemical and Environmental Sciences and Materials and Surface Science Institute, University of Limerick, Limerick, Ireland. E-mail: edmond.magner@ul.ie

Abstract

Dealloyed nanoporous gold (NPG) is a relatively new class of materials with potential applications in a wide range of fields, especially in electrochemistry. This review describes recent progress in the use of NPG electrodes for applications in bioelectrochemistry.

Keywords: nanoporous gold; glucose biosensor; electrochemistry; electron transfer

1. Introduction

Dealloyed nanoporous gold (NPG) is a porous material containing three dimensional frameworks of bicontinuous pores and ligaments, that is prepared by electro-/chemically dissolving the less noble component from Au alloys (Figure 1 and Figure 2A) [1]. For such materials to act as a support for enzymes, it is essential that the pore diameter sufficiently large to accommodate the enzyme and to enable effective transport of substrate to the enzyme. The pore sizes of NPG can be tailored in the range from ~5 to 700 nm [2] by tuning the composition of the alloy and the dealloying conditions [3]. NPG possesses advantages such as high surface-to-volume ratio, good electrical conductivity, chemical stability, biocompatibility and permeability [3]. NPG has been the subject of much attention for a range of applications including catalysis [4-6], optical sensing [7, 8] and analysis [9]. NPG electrodes have been used in the development of immunosensors [10-12], DNA sensors [13, 14], enzymatic biosensors [15, 16] and as enzyme-free sensors [17-19].

In this mini-review, we describe the use of dealloyed NPG for bioelectrochemical applications in biosensors and enzymatic biofuel cells. The review focuses on NPG fabricated via dealloying methods, rather than porous gold electrodes obtained with other methods (template methods etc.).

2. Dealloyed NPG fabrication and characterization

2.1 Fabrication

Corrosion processing of alloys with preferential removal of the less noble component (i.e. dealloying), originally known as “depletion gilding”, was established by the Indians of pre-Columbian Central America in order to create a layer of pure gold by etching copper from Cu/Au alloys [20]. Forty and Pickering showed that dealloying of a binary alloy resulted in a “spongy” morphology [20, 21]. In 2001, Erlebacher et al. demonstrated that the formation of pores was due to an intrinsic dynamic formation process [22, 23]. In the fabrication of NPG from

Ag/Au alloys, Ag atoms are dissolved under corrosive conditions such as concentrated nitric acid. At the solid/electrolyte interface, Au atoms aggregate into clusters and form islands rather than spreading over the surface, allowing the formation of pores. Subsequently, newly formed pores open up regions of virgin alloy for further etching of Ag, allowing the dealloying process to continue (Figure 2A).

According to the morphology of the precursor, dealloyed NPG can form nanoparticles [24], nanowires [25, 26], microwires [18] and films [3]. Bulk forms of NPG, such as wires and films are more convenient for manipulation. In 2004, Erlebacher et al. dealloyed commercially available 12-carat Ag/Au leaves (thickness of approximately 100 nm) to prepare crack-free NPG [3], which could be transferred and physically stabilized onto glassy carbon electrodes (GCEs) for further use (Figure 2B and C). NPG leaves mounted on GCE have been widely adopted for a range of electrochemical sensing applications [13, 17]. However, the electrodes are brittle and can become detached from the GCE over time [27]. A mechanically robust NPG can be prepared by sputtering a Ag/Au alloy onto a glass support with subsequent dealloying of Ag, which greatly facilitates their ease of use [27]. The multilayered system was comprised of a glass support, a ~10 nm thick Ti adhesion layer, a thin Au substrate layer (~35 nm) that improves adhesion and prevents delamination of the Ag/Au alloy layer during dealloying, and a ~100 nm thick $Ag_{67}Au_{33}$ alloy layer (Figure 2D). Magnetron sputtering enables various substrates (either conductive or non-conductive), variable alloy composition and pre-patterned deposition layers to be used. NPG can also be fabricated through reconstruction of Au electrode surfaces by applying alternative potential scans in a solution containing $ZnCl_2$ in solvents such as benzyl alcohol [28], dimethyl sulfoxide [29] and in ionic liquids [30, 31]. Zinc was first electrodeposited on Au to form a Zn/Au alloy at an elevated temperature during cathodic scanning. In the subsequent anodic potential scan, Zn was removed from the alloy, resulting in NPG (Figure 2E).

2.2 Characterization

The morphology (pore/ligament structure) and roughness of NPG are critical parameters for their successful utilisation. Microscopy techniques such as scanning or transmission electron microcopy (SEM/TEM) and atomic force microscopy (AFM) can be used to examine the morphology of NPG (Figure 1). For NPG with uniform pore-size-distribution and bicontinuous structures, the characteristic length scales (i.e. gold ligament width and pore channel diameter) can be determined by rotationally averaging the fast Fourier transform (FFT) power spectrum of a micrograph obtained by SEM or TEM [32]. TEM is particularly useful in characterizing surface modification of NPG (e.g. with nanoparticles or thin films) [33-35]. For example, modification of NPG by MnO_2 particles, thin films of tungsten sulfide, silica and conducting polymer can be clearly distinguished by TEM (Figure 3). The immobilisation of bovine serum albumin (BSA) and immunoglobulin G (IgG) on NPG has been examined using AFM [36], with individual features of proteins observed on the surface of the support. Electrochemical techniques, such as cyclic voltammetry (CV), are primarily applied to measure the electroactive surface areas (Figure 4). During potential cycling of NPG in sulfuric acid solution, anodic peaks between 1.1-1.4 V (vs. SCE) and a well-defined cathodic peak at ~0.9 V are obtained by oxidation and reduction of the outermost layer of gold atoms. The roughness factor R_f, can then be calculated, assuming that a specific charge of 390 μC cm^{-2} is required for gold oxide reduction

[37]. The measurement of the capacitance of the double-layer can also be used to determine the surface area [27]. Spectroscopic methods such as energy dispersive X-ray (EDX) spectroscopy and X-ray photoelectron spectroscopy (XPS) have been used to analyse the chemical composition the electrodes. XPS is useful for the analysis of NPG functionalized with biomolecules at relatively low concentrations [38, 39].

3. Properties of dealloyed NPG for bioelectrochemical applications

Porous gold electrodes can be fabricated using various routes that range from the hard template route [40-43], dynamic hydrogen bubble template method [44], to the anodization of gold electrodes [45] etc. The preparation of template-directed macroporous gold electrodes has been reviewed [46, 47]. Generally, hard template routes involve several steps: assembly of monodisperse spheres (e.g. polystyrene or silica with diameters ranging from 100 nm to 2 μm), electrodeposition of the metal and subsequent removal of the hard template (Figure 5A) [40]. This approach allows precise control the pore diameter and thickness of the porous structure, which are important parameters for bioelectrochemical applications [40, 48]. In the dynamic hydrogen bubble process, the hydrogen bubbles arising from the electrochemical reduction of H^+ act as templates for Au electrodeposition (Figure 5B) [44]. Anodization of Au takes place in an oxalate containing solution at a high potential (Figure 5C) [45], with the nanopores generated by the formation of a carbonaceous passivation film and its subsequent breakdown. Each route results in a porous gold material with specific morphology (Figure 5 and Table 1).

NPG obtained via dealloying methods possess a number of interesting features for applications in bioelectrochemistry. Four main points are summarized below:

Firstly, enzymes confined within NPG display higher stability on exposure to high temperatures [49, 50] and organic solvents [38] due to the nanopore providing a protective environment to the enzyme. After incubation at 50 °C for 2 h, only 6% of the initial activity of free laccase remained in comparison to 60% for laccase immobilised on NPG [49]. The activity of xylanase immobilised on NPG was assayed at 50 °C and exhibited only a 25% loss after 10 cycles [39]. After incubation for 30 minutes at 50, 60 and 70°C, 62, 59 and 54% of the initial activity was observed for free lipase, compared with 75, 74, and 76%, respectively, for lipase adsorbed on NPG (Figure 6A) [38]. After treatment with ethyl acetate (log *P* of 0.68), 27% of the initial activity of free lipase remained, while 81% activity was observed for the lipase-NPG biocomposite [38]. On exposure to chloroform (log *P* of 2.0) free and immobilised lipase retained 42 and 85% of the initial activity, respectively. After 20 cycles of treatment, the lipase-NPG biocomposite retained 33 and 38% of activity in ethyl acetate and chloroform, respectively.

Secondly, the high content of low index crystalline faces [51] on the surface of NPG (Figure 1G, H) can enhance the rate of electron transfer, enabling significantly enhanced electrochemical responses. Examples include glucose [52], hydrogen peroxide [17], nitrophenol [53], hydrazine [54], nitrite [55], etc. The electrocatalytic response to glucose and hydrogen peroxide is discussed in more detail in section 4.

Thirdly, thiol self-assembled monolayers (SAMs) are more stable on NPG than on planar Au electrodes [56, 57], as the monolayers benefit from the presence of defective sites, lattice strain and residual Ag on the ligament surface. In alkaline media, the peak potential for SAM desorption from dealloyed NPG occurred at a more negative potential (-1.15 V vs. SCE) versus that observed at planar gold (-0.74 V) [56], indicative of a stronger Au-S bond.

Fourthly, NPG can exclude large proteins from accessing the internal pores, reducing the effects of biofouling [58, 59]. In the presence of 2 mg mL^{-1} of BSA [58], the time for the initial electrochemical response of $[Fe(CN)_6]^{3-}$ to decrease by 50% was 3 min on planar gold, 12 min on macroporous gold (1200 nm pore network, obtained via hard templating of latex spheres), and 38 min on hierarchical gold (1200/60 nm bimodal pore network). In contrast, at dealloyed NPG (~5–50 nm pore, R_f of 15), the current decreased by ca. 12% after 60 mi, indicative of a significant resistance to fouling. On exposure to a solution of fibrinogen (1 mg mL^{-1}) for two hours [60], the faradaic peak associated with the oxidation of ascorbic acid disappeared at planar gold electrodes but remained at NPG. Collectively, the voltammetric response to $[Fe(CN)_6]^{3-}$ and ascorbic acid, displaying fast and slow ET kinetics, respectively, was sensitive to surface contamination at planar gold but was significantly less affected at NPG.

4. Glucose biosensors

4.1 Enzyme based glucose biosensors

The first glucose biosensor utilised glucose oxidase (GOx) immobilised on a platinum electrode [61]. The majority of commercially available glucose biosensors utilise GOx due to its relatively low price, high selectivity and stability [62, 63]. GOx is a flavoprotein that catalyses the oxidation of β-D-glucose to D-glucono-δ-lactone, which is then hydrolyzed to gluconic acid [64]. The redox active group in GOx, flavine adenine dinucucleotide (FAD), is concomitantly reduced to $FADH_2$. GOx(FAD) can be regenerated using molecular oxygen, electron mediators or directly at the electrode surface. Electron transfer (ET) can occur via mediated (MET) or direct ET (DET). The latter process has the advantages that it avoids possible leakage and diffusional limitations associated with the use of mediators. However, the redox active centers of GOx are deeply buried with a minimal distance of 13-18 Å between the periphery of GOx and the N7 nitrogen of the isoalloxazine rings of FAD [65]. Achieving DET of GOx (third-generation glucose biosensors [63]) has been hampered by requirements including optimization of enzyme orientation and minimization of the distance between the active center of the enzyme and the surface of the electrode .

When oxygen is used as a mediator, hydrogen peroxide generated in the process can be detected via either oxidation or reduction. A potential of +0.7 V (vs. SCE) is required in order to observe a faradaic response to H_2O_2 at planar gold electrodes, a rather high detection potential which may cause interference from other species. In contrast, NPG can oxidize H_2O_2 at an onset potential of +0.2 V (vs. SCE) and a peak potential of +0.4 V (vs. SCE) [66]. According to Erlebacher et al. [67], the primary reason that NPG displays a higher catalytic activity than planar gold towards the reduction or oxidation of H_2O_2 is due to the higher concentration of steps on NPG (Figure 1G, H). A glucose biosensor has been developed by physical adsorption of GOx within the NPG followed by covering the electrode with a Nafion film. The electrode displayed a linear range up

to 18 mM, a sensitivity of 0.7 μA cm^{-2} mM^{-1} and a detection limit of 196 μM (applied potential +0.4 V vs. SCE) [66]. The reduction of H_2O_2 at NPG occurs at an onset potential of -0.1 V (vs. Ag/AgCl) [15, 17]. Responses to H_2O_2 reduction at NPG with pore sizes of 18, 30, 40 and 50 nm have been compared, and the electrodes with smaller pores yielded higher sensitivity, arising from the larger surface area of these electrodes. After immobilisation of GOx via thiol linking and at an applied potential of -0.2 V (Ag/AgCl), the highest sensitivity (8.6 μA cm^{-2} mM^{-1}) to glucose was obtained from NPG electrodes with pore sizes of 30 nm [15], suggesting that the small pores of 18 nm NPG were not sufficiently large to accommodate higher amounts of enzyme. Prussian Blue (PB) was electrodeposited onto NPG for enhanced activity to H_2O_2 reduction [68]. At a potential of 0 V (vs. Ag/AgCl), a linear response up to 30 mM glucose with a sensitivity of 50 μA cm^{-2} mM^{-1}, as well low levels of interference from lactate, uric acid and ascorbic acid was obtained.

Mediators such as p-benzoquinone (BQ) and ferrocenecarboxylic acid (FCA) have been used to oxidise GOx immobilised on NPG electrodes (Figure 6B) [69, 70]. In the presence of mediators that undergo diffusion controlled and fast kinetic redox reactions, the enzymes immobilised deeply inside the NPG electrode do not contribute to the detection of glucose, as the redox reaction occurs at the external regions of the pores. Redox couples that display with fast heterogeneous kinetics, such as $[Fe(CN)_6]^{4-/3-}$ and $[Ru(NH_3)^6]^{3-/2-}$, show similar responses on NPG [27]. Electrodes utilising such mediators do not display significant increases in the current, similarly, diffusional limitations arising from substrate diffusion to enzyme molecules within the pores results in responses that are similar to those obtained on planar supports.

In the presence of excess levels of mediator, the sensitivity of a sensor is determined by the amount of accessible immobilised enzymes [69]. Entrapment is one way to increase enzyme loading. One-step electropolymerization of a hybrid film of poly(3,4-ethylenedioxythiophene) (PEDOT) and GOx on nanoporous gold (NPG) has been described (Figure 6C) [33]. Using BQ as a mediator, the biosensor, exhibited a sensitivity of 7.3 μA cm^{-2} mM^{-1} and a linear response over the concentration range 0.1-15 mM. Redox hydrogel "wired" glucose oxidase been very successful in the development of glucose monitoring technology [71, 72]. By enveloping the redox enzymes with redox polymers, electron communication of redox centers of enzymes and polymers with electrode surfaces can be established [73]. Encapsulation of GOx within Os-redox polymer onto NPG has been employed as a glucose biosensor (with a detection limit of 2.0 (±0.1) μM [74]), and for a glucose/O_2 biofuel cell [75]. Drop casting of redox hydrogel/enzyme mixture onto porous electrodes generally leads to a "cap" like configuration [76], which hampers the full occupancy of deeper pores. Electrodeposition of a redox polymer is recommended to enable the generation of a stable and uniformly distributed film [77].

The nicotinamide adenine dinucleotide (NAD) dependent enzyme glucose dehydrogenase (GDH) is also used for the detection of glucose s The oxidation of NADH requires a high overpotential [78]. NPG can enhance the sluggish ET kinetics of NADH oxidation [66], with a peak potential for the oxidation of NADH of +0.52 V (vs. SCE), while +0.72 V on planar gold. Alcohol dehydrogenase (ADH) modified NPG electrodes can operate at an applied potential of +0.5 V (vs. SCE) for the detection of ethanol [66], though this potential is still high for many practical

applications. The flavocytochrome cellobiose dehydrogenase (CDH) can be utilised in the development of third-generation glucose biosensors [79]. CDH processes two separate domains connected via a polypeptide linker region. The flavodehydrogenase domain is catalytically active and the cytochrome domain with a haem b group acts as an electron relay, i.e. built-in mediator. This dual-domain feature enables efficient DET between the active site of the enzyme and the electrode surface. NPG modified with SAMs of 1-thioglycerol can promote the DET of *Corynascus thermophiles* CDH (*Ct*CDH) [80]. *Ct*CDH immobilised with an Os-redox polymer on NPG displayed a limit of detection of 16 (±0.1) μM for the determination of glucose [74]. The main constraint of CDH for blood glucose sensing is its promiscuous characteristic since it is capable of catalysing several carbohyrates. However, it may be useful in the analysis of glucose in samples where glucose is present in much higher concentrations.

Practical application of glucose biosensors requires testing in real samples including blood, serum or other human body fluids (e.g. saliva, urine and sweat). However, operation in blood or serum results in fouling of the electrode arising from protein adsorption on the electrode surface, leading to a decreased sensor response [81]. As already mentioned, the voltammetric response of $[Fe(CN)_6]^{3-}$ in phosphate buffer containing 2 mg mL^{-1} of BSA was stable on NPG for 22 hours but not on a planar gold electrode [58]. Glucose biosensors should be capable of operating in whole blood samples [82]. To date, NPG based biosensors are mostly tested in 10-100 fold diluted serum [12, 70, 83, 84].

.

4.2 Nonenzymatic glucose biosensors

The development of numerous nonenzymatic glucose sensors, based on direct electrooxidation of glucose, has been described [85]. NPG is promising as it can promote the relatively sluggish kinetics of glucose oxidation and its high specific surface area is less prone to interference from ascorbic acid and uric acid. Au-OH_{ads} layers, formed by adsorption of OH^- on gold electrodes in a neutral or alkaline solution act as "pre-oxidation precursors" and are active in the oxidation of glucose at low potentials [86]. The reaction pathways are shown in equations (1) to (4) [52, 87]:

$$Au + OH^- \rightarrow Au - OH_{ads}^{(1-\lambda)-} + \lambda e^- \quad (1)$$

In neutral media:

$$Au - OH_{ads} + Glu\cos e \rightarrow Gluconolactone + Au + e^- + H_2O + H^+ \quad (2)$$

In neutral media:

$$Au - OH_{ads} + Glu\cos e + OH^- \rightarrow Gluconolactone + Au + e^- + 2H_2O \quad (3)$$

$$Gluconolactone \rightarrow Gluconic\ acid\ (hydrolysis) \quad (4)$$

The presence of residual amounts of Ag on NPG significantly enhances the electrooxidation of glucose in alkaline solutions, as Ag promotes the chemisorption of OH^- at active Au atoms [52]. In 0.1 M NaOH, planar gold displayed an onset potential of -0.6 V (vs. SCE) for glucose oxidation, while -0.9 V (vs. SCE) for NPG with 12 nm pores [88]. The catalytic current density of NPG with 12 nm pores was over 1.5 and 17 times higher than that of NPG with 35 nm pores

and planar gold. Similar pore size effects can be seen when working in neutral pH, with a sensitivity of 20.1μA cm^{-2} mM^{-1} and linear range up to 18 mM. NPG with 18 nm pores gave rise to an improved response to glucose in comparison to NPGs with pores of 30, 40 and 50 nm in size [89]. Poisoning of NPG by the irreversible adsorption of chloride ions can occur [89]. To address this issue, a thin film (~5 nm) of CuO has been electrodeposited onto NPG with a sensitivity of 374 μA cm^{-2} mM^{-1} towards glucose and a linear range up to 12 mM obtained operation in alkaline media [90].

By decorating NPG wires with cobalt oxide, the resultant nonenzymatic glucose biosensor had a high sensitivity (2500 μA cm^{-2} mM^{-1}) and a low detection limit of 5 nM [18]. In both metal oxide modification cases (NPG/CuO and NPG/Co_3O_4), however, no response to glucose was observed at neutral pH. Thus dilution of serum samples in alkaline media is generally required [90]. Although there have been a wide range of publications on the use of transition metal oxides as the basis for nonenzymatic glucose sensors, their applications for the determination of glucose concentration are limited due to their lack of specificity and the need to operate in alkaline media. Direct oxidation of glucose with inorganic catalysts, coupled with a Pt based cathode for oxygen reduction, are more applicable in alkaline glucose fuel cells or enzyme-free (abiotic) glucose fuel cells [91, 92].

5. Bioelectrochemical applications of NPG

5.1 Heme-proteins

Cytochrome c (*cyt c*) is a model protein that can undergo DET at SAM modified. The topography of gold electrodes were shown to play an important role in the adsorption and electrochemical response of *cyt c* [93]. Various substrates with different surface roughness including evaporated, bulk, single crystal, and epitaxially grown gold on mica were studied. On a Au electrode with smoother surface, SAMs exhibited an increased ability to block a diffusing probe molecule, implying a lower level of defectiveness. Moreover, the extent of adsorption and the electrochemical response of the adsorbed cyt c decreased significantly on smooth substrates. Thus, rough gold surfaces, resulting in SAMs with a high degree of defects, were more suitable for the optimal faradaic response [93]. Well-defined, nearly symmetric voltammograms (peak separation ΔE_p of 18±1 mV) were obtained by covalently attaching *cyt c* on NPG modified with a mixed SAM [27]. The surface coverage of active *cyt c* on a NPG electrode (R_f of 28) was ~11 times higher than that achieved at a planar Au surface. The adsorbed proteins were stable and no decreases in the voltammetric response with continuous potential cycling (30 scans) in aqueous buffer were observed.

5.2 Multi-copper oxidases

Multi-copper oxidases (MCOs, e.g. laccase and bilirubin oxidase (BOD)) modified electrodes have been extensively employed as cathodes of enzymatic biofuel cells (BFC) [94], which are of significant interest due to their potential applications as autonomous power suppliers [95, 96]. Generally, MCOs contain four copper atoms: the T1 copper site acts as an electron acceptor while O_2 is reduced to H_2O at the T2/T3 copper sites [97]. NPG based BFCs have been constructed based on GOx or CDH at the anodes and laccase or BOD at the cathode [57, 74, 75]. The electrodes displayed improved power densities and stabilities in comparison to planar

electrodes. For example, glucose/O_2 BFCs operating via mediated ET at a GOx anode and BOD cathode, displayed maximum power densities of 35 vs. 11 μW cm^{-2} in 100 mM glucose at osmium polymer-modified nanoporous and planar gold (Figure 7), respectively [74]. Using GOx and laccase with Os redox polymers [98], maximum power densities of 17 and 38 μW cm^{-2} were obtained on planar gold and 2½ sphere gold macroporous electrodes, respectively.

Trametes hirsute laccase (ThLc) showed well-defined DET at unmodified NPG electrodes, in contrast to the absence of a response at unmodified polycrystalline gold electrodes [99]. The significant response of laccase obtained on NPG was proposed to arise from preferential orientation of enzymes onto the surface of NPG, decreasing the distance for ET to the T1 copper sites. On covering the electrode with an epoxy cap, significantly higher currents (by a factor of 10) were obtained. Higher responses were obtained when the temperature was increased from 20 to 37 °C. The current obtained from DET was 30% of that observed for ThLc co-immobilised with an osmium redox polymer, indicating that higher amounts of enzyme are electrochemically addressable in the presence of the redox polymer. Moreover, pore size dependent performance has also observed when laccase was physically adsorbed on different NPG surfaces (10-20 nm, 40-50 nm and 90-100 nm, a larger pore size typically refers to smaller surface area) [49]. A pore size of 40-50 nm resulted in the largest amount of immobilised laccase, as mass transport of the enzyme to the inner pores was limited. A layer-by-layer assembly of AuNPs and laccase onto ordered macroporous gold electrodes enabled the DET of laccase, with a formal potential of 0.25 V vs. Ag/AgCl, which was very close to the theoretical value for the T2 copper site (0.21 V) [100].

Previous reports have described DET of BOD on bare or negatively charged SAMs modified single-crystal electrodes [101] and three-dimensional AuNP electrodes [102]. BOD was physically embedded into bare NPG and the resulted electrodes displayed bioelectrocatalytic reduction of molecular oxygen, undergoing efficient DET (Figure 8) [76]. However, BOD was relatively loosely bound and easily removed from the surface of the electrode as only 50% of potential scan was retained in second scan. On coating the electrode with an epoxy film by creating covalent bonds with nucleophilic groups such as amine, thiol and hydroxyl groups on the surface of the enzyme, current densities were stable on repeated potential scans. As a result, a minimal inhibition of F^- with ca. 3.5% activity loss was achieved on a biocathode stabilized with epoxy, indicating the exclusion of F^- from the pores by the polymer and also the confinement of the enzyme in the pores of the electrode in a manner which precludes binding of F^- to the T2/T3 site.

6. Conclusions and prospects

Nanoporous gold has emerged as a promising support for the immobilisation of enzymes for bioelectrochemical applications (i.e. biosensors and biofuel cells) with improved response and stability. The porous nature of the support enables the immobilisation of high amounts of enzyme, though such loadings may not be of benefit for very deep pores where diffusion of enzyme substrate into the pores can become rate limiting. The use of flow systems can enhance substrate transport and overcome such limitations. A micro-fluidic device utilising NPG is promising due to its potential advantages of miniaturisation, integration and high-performance. NPG can be

deposited on plastic supports for flexible devices, enabling the development of thin flexible polymer-based electronic devices, for example, that are integrated with “smart” contact lenses for biomedical applications [103].

Acknowledgements

The National Natural Science Foundation of China (NSFC No. 51301096), Shandong Provincial Natural Science Foundation (ZR2013EMQ012) and the Fundamental Research Funds of Shandong University (No. 2014JC017) are appreciated by P. Si. The European Commission (FP7-PEOPLE-2013-ITN 607793 “Bioenergy”) and Government of Ireland Postgraduate Scholarship (GOIPG/2014/659) are greatly acknowledged by X. Xiao. Assoc. Prof. Jingdong Zhang and Prof. Yi Ding are appreciated for their kind support and meaningful discussions. We thank Dr. Urszula Salaj-Kosla for reading the manuscript.

References

[1] A. Wittstock, J. Biener, J. Erlebacher, Nanoporous Gold: From an Ancient Technology to a High-tech Material, RSC Publishing 2012.

[2] L. Qian, X. Yan, T. Fujita, A. Inoue, M. Chen, Surface enhanced Raman scattering of nanoporous gold: Smaller pore sizes stronger enhancements, Appl. Phys. Lett., 90 (2007) 153120-153120.

[3] Y. Ding, Y.J. Kim, J. Erlebacher, Nanoporous Gold Leaf: “Ancient Technology”/Advanced Material, Adv. Mater., 16 (2004) 1897–1900.

[4] X. Zhang, Y. Ding, Unsupported nanoporous gold for heterogeneous catalysis, Catal. Sci. Technol., 3 (2013) 2862-2868.

[5] A.W. Arne Wittstock, Marcus Bäumer, Nanoporous Gold as a Platform for a Building Block Catalyst, ACS Catal., 2 (2012) 2199-2215.

[6] J. Biener, M.M. Biener, R.J. Madix, C.M. Friend, Nanoporous Gold: Understanding the Origin of the Reactivity of a 21st Century Catalyst Made by Pre-Columbian Technology, ACS Catal., (2015) 6263-6270.

[7] Y. Ding, M. Chen, Nanoporous metals for catalytic and optical applications, MRS Bull., 34 (2009) 569-576.

[8] L. Zhang, H. Chang, A. Hirata, H. Wu, Q.-K. Xue, M. Chen, Nanoporous Gold Based Optical Sensor for Sub-ppt Detection of Mercury Ions, ACS Nano, 7 (2013) 4595-4600.

[9] M.M. Collinson, Nanoporous gold electrodes and their applications in analytical chemistry, ISRN Anal. Chem., 2013 (2013) 1-21.

[10] C. Ding, H. Li, K. Hu, J.-M. Lin, Electrochemical immunoassay of hepatitis B surface antigen by the amplification of gold nanoparticles based on the nanoporous gold electrode, Talanta, 80 (2010) 1385-1391.

[11] Q. Wei, Y. Zhao, C. Xu, D. Wu, Y. Cai, J. He, H. Li, B. Du, M. Yang, Nanoporous gold film based immunosensor for label-free detection of cancer biomarker, Biosens. Bioelectron., 26 (2011) 3714-3718.

[12] M. Li, M. Zhang, S. Ge, M. Yan, J. Yu, J. Huang, S. Liu, Ultrasensitive electrochemiluminescence immunosensor based on nanoporous gold electrode and Ru-AuNPs/graphene as signal labels, Sens. Actuat. B: Chem., 181 (2013) 50-56.

[13] K. Hu, D. Lan, X. Li, S. Zhang, Electrochemical DNA biosensor based on nanoporous gold electrode and multifunctional encoded DNA− Au bio bar codes, Anal. Chem., 80 (2008) 9124-9130.

[14] P. Daggumati, Z. Matharu, L. Wang, E. Seker, Biofouling-Resilient Nanoporous Gold Electrodes for DNA Sensing, Anal. Chem., 87 (2015) 8618-8622.
[15] L.Y. Chen, T. Fujita, M.W. Chen, Biofunctionalized nanoporous gold for electrochemical biosensors, Electrochim. Acta, 67 (2012) 1-5.
[16] C. Wu, H. Sun, Y. Li, X. Liu, X. Du, X. Wang, P. Xu, Biosensor based on glucose oxidase-nanoporous gold co-catalysis for glucose detection, Biosens. Bioelectron., 66 (2015) 350-355.
[17] F. Meng, X. Yan, J. Liu, J. Gu, Z. Zou, Nanoporous gold as non-enzymatic sensor for hydrogen peroxide, Electrochim. Acta, 56 (2011) 4657-4662.
[18] X.-Y. Lang, H.-Y. Fu, C. Hou, G.-F. Han, P. Yang, Y.-B. Liu, Q. Jiang, Nanoporous gold supported cobalt oxide microelectrodes as high-performance electrochemical biosensors, Nat. Commun., 4 (2013) 2169.
[19] C. Xiao, Y.-L. Liu, J.-Q. Xu, S.-W. Lv, S. Guo, W.-H. Huang, Real-time monitoring of H2O2 release from single cells using nanoporous gold microelectrodes decorated with platinum nanoparticles, Analyst, 140 (2015) 3753-3758.
[20] A.J. Forty, Corrosion micromorphology of noble metal alloys and depletion gilding, Nature, 282 (1979) 597-598.
[21] H.W. Pickering, C. Wagner, Electrolytic Dissolution of Binary Alloys Containing a Noble Metal, J. Electrochem. Soc., 114 (1967) 698-706.
[22] J. Erlebacher, M.J. Aziz, A. Karma, N. Dimitrov, K. Sieradzki, Evolution of nanoporosity in dealloying, Nature, 410 (2001) 450-453.
[23] J. Erlebacher, An atomistic description of dealloying porosity evolution, the critical potential, and rate-limiting behavior, J. Electrochem. Soc., 151 (2004) C614-C626.
[24] X. Li, Q. Chen, I. McCue, J. Snyder, P. Crozier, J. Erlebacher, K. Sieradzki, Dealloying of Noble-Metal Alloy Nanoparticles, Nano Lett., 14 (2014) 2569-2577.
[25] Z. Liu, P.C. Searson, Single Nanoporous Gold Nanowire Sensors, J. Phys. Chem. B, 110 (2006) 4318-4322.
[26] X. Gu, X. Cong, Y. Ding, Platinum-Decorated Au Porous Nanotubes as Highly Efficient Catalysts for Formic Acid Electro-Oxidation, ChemPhysChem, 11 (2010) 841-846.
[27] M.D. Scanlon, U. Salaj-Kosla, S. Belochapkine, D. MacAodha, D. Leech, Y. Ding, E. Magner, Characterization of nanoporous gold electrodes for bioelectrochemical applications, Langmuir, 28 (2011) 2251-2261.
[28] F. Jia, C. Yu, Z. Ai, L. Zhang, Fabrication of Nanoporous Gold Film Electrodes with Ultrahigh Surface Area and Electrochemical Activity, Chem. Mater., 19 (2007) 3648-3653.
[29] H. Dong, X. Cao, Nanoporous Gold Thin Film: Fabrication, Structure Evolution, and Electrocatalytic Activity, J. Phys. Chem. C, 113 (2009) 603-609.
[30] L. Lu, Y. Dong, J. Wang, Q. Li, X. Wu, Direct electrochemistry and bioelectrocatalysis of horseradish peroxidase entrapped in a self-supporting nanoporous gold electrode: a new strategy to improve the orientation of immobilized enzymes, Anal. Methods, 7 (2015) 6686-6694.
[31] J. F. Huang, B. T. Lin, Application of a nanoporous gold electrode for the sensitive detection of copper via mercury-free anodic stripping voltammetry, Analyst, 134 (2009) 2306-2313.
[32] F. Takeshi, C. Ming Wei, Characteristic Length Scale of Bicontinuous Nanoporous Structure by Fast Fourier Transform, Jpn. J. Appl. Phys., 47 (2008) 1161.
[33] X. Xiao, M.e. Wang, H. Li, P. Si, One-step fabrication of bio-functionalized nanoporous

gold/poly (3, 4-ethylenedioxythiophene) hybrid electrodes for amperometric glucose sensing, Talanta, 115 (2013) 1054-1059.
[34] X. Xiao, C. Engelbrekt, Z. Li, P. Si, Hydrogen evolution at nanoporous gold/tungsten sulfide composite film and its optimization, Electrochim. Acta, 173 (2015) 393-398.
[35] X. Lang, A. Hirata, T. Fujita, M. Chen, Nanoporous metal/oxide hybrid electrodes for electrochemical supercapacitors, Nat. Nanotechnol., 6 (2011) 232–236.
[36] Y.H. Tan, J.R. Schallom, N.V. Ganesh, K. Fujikawa, A.V. Demchenko, K.J. Stine, Characterization of protein immobilization on nanoporous gold using atomic force microscopy and scanning electron microscopy, Nanoscale, 3 (2011) 3395-3407.
[37] S. Trasatti, O. A. Petrii, Real surface area measurements in electrochemistry, Pure Appl. Chem., 63 (1991) 711-734.
[38] X. Wang, X. Y. Liu, X. L. Yan, P. Zhao, Y. Ding, P. Xu, Enzyme-Nanoporous Gold Biocomposite: Excellent Biocatalyst with Improved Biocatalytic Performance and Stability, PLoS ONE, 6 (2011) e24207.
[39] X. Yan, X. Wang, P. Zhao, Y. zhang, P. Xu, Y. Ding, Xylanase immobilized nanoporous gold as a highly active and stable biocatalyst, Micropor. Mesopor. Mater., 161 (2012) 1-6.
[40] R. Szamocki, S. Reculusa, S. Ravaine, P. N. Bartlett, A. Kuhn, R. Hempelmann, Tailored Mesostructuring and Biofunctionalization of Gold for Increased Electroactivity, Angew. Chem. Int. Edit., 45 (2006) 1317–1321.
[41] R. Szamocki, A. Velichko, C. Holzapfel, F. Mücklich, S. Ravaine, P. Garrigue, N. Sojic, R. Hempelmann, A. Kuhn, Macroporous ultramicroelectrodes for improved electroanalytical measurements, Anal. Chem., 79 (2007) 533-539.
[42] P.N. Bartlett, J.J. Baumberg, P.R. Birkin, M.A. Ghanem, M.C. Netti, Highly Ordered Macroporous Gold and Platinum Films Formed by Electrochemical Deposition through Templates Assembled from Submicron Diameter Monodisperse Polystyrene Spheres, Chem. Mater., 14 (2002) 2199-2208.
[43] M. Heim, S. Reculusa, S. Ravaine, A. Kuhn, Engineering of complex macroporous materials through controlled electrodeposition in colloidal superstructures, Adv. Funct. Mater., 22 (2012) 538-545.
[44] H. du Toit, M. Di Lorenzo, Continuous power generation from glucose with two different miniature flow-through enzymatic biofuel cells, Biosens. Bioelectron., 69 (2015) 199-205.
[45] K. Nishio, H. Masuda, Anodization of gold in oxalate solution to form a nanoporous black film, Angew. Chem. Int. Edit., 50 (2011) 1603-1607.
[46] A. Walcarius, A. Kuhn, Ordered porous thin films in electrochemical analysis, TrAC, Trends Anal. Chem., 27 (2008) 593-603.
[47] A. Walcarius, Template-directed porous electrodes in electroanalysis, Anal. Bioanal. Chem., 396 (2010) 261-272.
[48] R. Szamocki, A. Velichko, F. Mücklich, S. Reculusa, S. Ravaine, S. Neugebauer, W. Schuhmann, R. Hempelmann, A. Kuhn, Improved enzyme immobilization for enhanced bioelectrocatalytic activity of porous electrodes, Electrochem. Commun., 9 (2007) 2121-2127.
[49] H. Qiu, C. Xu, X. Huang, Y. Ding, Y. Qu, P. Gao, Adsorption of Laccase on the Surface of Nanoporous Gold and the Direct Electron Transfer between Them, J. Phys. Chem. C, 112 (2008) 14781-14785.
[50] M. Hakamada, M. Takahashi, M. Mabuchi, Enhanced thermal stability of laccase immobilized on

monolayer-modified nanoporous Au, Mater. Lett., 66 (2012) 4-6.
[51] T. Fujita, P. F. Guan, K. McKenna, X. Y. Lang, A. Hirata, L. Zhang, T. Tokunaga, S. Arai, Y. Yamamoto, N. Tanaka, Y. Ishikawa, N. Asao, Y. Yamamoto, J. Erlebacher, M. W. Chen, Atomic origins of the high catalytic activity of nanoporous gold, Nat. Mater., 11 (2012) 775–780.
[52] Z. Liu, L. Huang, L. Zhang, H. Ma, Y. Ding, Electrocatalytic oxidation of d-glucose at nanoporous Au and Au–Ag alloy electrodes in alkaline aqueous solutions, Electrochim. Acta, 54 (2009) 7286-7293.
[53] Z. Liu, J. Du, C. Qiu, L. Huang, H. Ma, D. Shen, Y. Ding, Electrochemical sensor for detection of *p*-nitrophenol based on nanoporous gold, Electrochem. Commun., 11 (2009) 1365-1368.
[54] X. Yan, F. Meng, S. Cui, J. Liu, J. Gu, Z. Zou, Effective and rapid electrochemical detection of hydrazine by nanoporous gold, J. Electroanal. Chem., 661 (2011) 44-48.
[55] X. Ge, L. Wang, Z. Liu, Y. Ding, Nanoporous Gold Leaf for Amperometric Determination of Nitrite, Electroanalysis, 23 (2011) 381-386.
[56] M. Hakamada, M. Takahashi, T. Furukawa, K. Tajima, K. Yoshimura, Y. Chino, M. Mabuchi, Electrochemical stability of self-assembled monolayers on nanoporous Au, Phys. Chem. Chem. Phys., 13 (2011) 12277-12284.
[57] M. Hakamada, M. Takahashi, M. Mabuchi, Enzyme electrodes stabilized by monolayer-modified nanoporous Au for biofuel cells, Gold Bull., 45 (2012) 9-15.
[58] J. Patel, L. Radhakrishnan, B. Zhao, B. Uppalapati, R.C. Daniels, K.R. Ward, M.M. Collinson, Electrochemical Properties of Nanostructured Porous Gold Electrodes in Biofouling Solutions, Anal. Chem., 85 (2013) 11610-11618.
[59] S. Saraf, C.J. Neal, S. Park, S. Das, S. Barkam, H.J. Cho, S. Seal, Electrochemical study of nanoporous gold revealing anti-biofouling properties, RSC Adv., 5 (2015) 46501-46508.
[60] A.A. Farghaly, M. Lam, C.J. Freeman, B. Uppalapati, M.M. Collinson, Potentiometric Measurements in Biofouling Solutions: Comparison of Nanoporous Gold to Planar Gold, J. Electrochem. Soc., 163 (2016) H3083-H3087.
[61] L.C. Clark, C. Lyons, Electrode systems for continuous monitoring in cardiovascular surgery, Ann. Ny. Acad. Sci., 102 (1962) 29-45.
[62] R. Wilson, A. P. F. Turner, Glucose oxidase: an ideal enzyme, Biosens. Bioelectron., 7 (1992) 165-185.
[63] J. Wang, Electrochemical Glucose Biosensors, Chem. Rev., 108 (2008) 814–825.
[64] S.B. Bankar, M.V. Bule, R.S. Singhal, L. Ananthanarayan, Glucose oxidase — An overview, Biotechnol. Adv, 27 (2009) 489-501.
[65] H.J. Hecht, D. Schomburg, H. Kalisz, R.D. Schmid, The 3D structure of glucose oxidase from *Aspergillus niger*. Implications for the use of GOD as a biosensor enzyme, Biosens. Bioelectron., 8 (1993) 197-203.
[66] H. Qiu, L. Xue, G. Ji, G. Zhou, X. Huang, Y. Qu, P. Gao, Enzyme-modified nanoporous gold-based electrochemical biosensors, Biosens. Bioelectron., 24 (2009) 3014-3018.
[67] R. Zeis, T. Lei, K. Sieradzki, J. Snyder, J. Erlebacher, Catalytic reduction of oxygen and hydrogen peroxide by nanoporous gold, J. Catal., 253 (2008) 132-138.
[68] T. Li, F. Jia, Y. Fan, Z. Ding, J. Yang, Fabrication of nanoporous thin-film working electrodes and their biosensingapplications, Biosens. Bioelectron., 42 (2013) 5-11.
[69] X. Xiao, J. Ulstrup, H. Li, J. Zhang, P. Si, Nanoporous gold assembly of glucose oxidase for electrochemical biosensing, Electrochim. Acta, 130 (2014) 559-567.

[70] X. Xiao, H. Li, K. Zhang, P. Si, Examining the effects of self-assembled monolayers on nanoporous gold based amperometric glucose biosensors, Analyst, 139 (2014) 488-494.
[71] A. Heller, Electrical connection of enzyme redox centers to electrodes, J. Phys. Chem., 96 (1992) 3579-3587.
[72] A. Heller, B. Feldman, Electrochemical Glucose Sensors and Their Applications in Diabetes Management, Chem. Rev., 108 (2008) 2482-2505.
[73] A. Heller, Electron-conducting redox hydrogels: design, characteristics and synthesis, Curr. Opin. Chem. Biol., 10 (2006) 664-672.
[74] U. Salaj-Kosla, M.D. Scanlon, T. Baumeister, K. Zahma, R. Ludwig, P.Ó. Conghaile, D. MacAodha, D. Leech, E. Magner, Mediated electron transfer of cellobiose dehydrogenase and glucose oxidase at osmium polymer-modified nanoporous gold electrodes, Anal. Bioanal. Chem., 405 (2013) 3823-3830.
[75] X. Xiao, E. Magner, A biofuel cell in non-aqueous solution, Chem. Commun., 51 (2015) 13478-13480.
[76] U. Salaj-Kosla, S. Pöller, Y. Beyl, M.D. Scanlon, S. Beloshapkin, S. Shleev, W. Schuhmann, E. Magner, Direct electron transfer of bilirubin oxidase (*Myrothecium verrucaria*) at an unmodified nanoporous gold biocathode, Electrochem. Commun., 16 (2012) 92-95.
[77] Z. Gao, G. Binyamin, H.H. Kim, S.C. Barton, Y. Zhang, A. Heller, Electrodeposition of Redox Polymers and Co-Electrodeposition of Enzymes by Coordinative Crosslinking, Angew. Chem. Int. Ed., 41 (2002) 810-813.
[78] F.D. Munteanu, N. Mano, A. Kuhn, L. Gorton, Mediator-modified electrodes for catalytic NADH oxidation: high rate constants at interesting overpotentials, Bioelectrochemistry, 56 (2002) 67-72.
[79] R. Ludwig, R. Ortiz, C. Schulz, W. Harreither, C. Sygmund, L. Gorton, Cellobiose dehydrogenase modified electrodes: advances by materials science and biochemical engineering, Anal. Bioanal. Chem., 405 (2013) 3637-3658.
[80] U. Salaj-Kośla, Nanoporous gold electrodes as matrices for enzyme immobilization for application in biosensors and biofuel cells, PhD thesis, University of Limerick, Limerick, Ireland, 2012.
[81] A. Barfidokht, J.J. Gooding, Approaches Toward Allowing Electroanalytical Devices to be Used in Biological Fluids, Electroanalysis, 26 (2014) 1182-1196.
[82] E. Magner, Detection of ferricyanide as a probe for the effect of hematocrit in whole blood biosensors, Analyst, 126 (2001) 861-865.
[83] S. Ge, X. Jiao, D. Chen, Ultrasensitive electrochemical immunosensor for CA 15-3 using thionine-nanoporous gold-graphene as a platform and horseradish peroxidase-encapsulated liposomes as signal amplification, Analyst, 137 (2012) 4440-4447.
[84] C. Wu, X. Liu, Y. Li, X. Du, X. Wang, P. Xu, Lipase-nanoporous gold biocomposite modified electrode for reliable detection of triglycerides, Biosens. Bioelectron., 53 (2014) 26-30.
[85] C. Chen, Q. Xie, D. Yang, H. Xiao, Y. Fu, Y. Tan, S. Yao, Recent advances in electrochemical glucose biosensors: a review, RSC Adv., 3 (2013) 4473-4491.
[86] M.W. Hsiao, R.R. Adžić, E.B. Yeager, Electrochemical Oxidation of Glucose on Single Crystal and Polycrystalline Gold Surfaces in Phosphate Buffer, J. Electrochem. Soc., 143 (1996) 759-767.
[87] S.B. Aoun, Z. Dursun, T. Koga, G.S. Bang, T. Sotomura, I. Taniguchi, Effect of metal ad-layers on Au(1 1 1) electrodes on electrocatalytic oxidation of glucose in an alkaline solution, J. Electroanal. Chem., 567 (2004) 175-183.

[88] Q. Li, S. Cui, X. Yan, Electrocatalytic oxidation of glucose on nanoporous gold membranes, J. Solid State Electrochem., 16 (2012) 1099-1104.
[89] L. Y. Chen, X. Y. Lang, T. Fujita, M. W. Chen, Nanoporous gold for enzyme-free electrochemical glucose sensors, Scripta. Mater., 65 (2011) 17-20.
[90] X. Xiao, M.e. Wang, H. Li, Y. Pan, P. Si, Non-enzymatic glucose sensors based on controllable nanoporous gold/copper oxide nanohybrids, Talanta, 125 (2014) 366-371.
[91] S. Kerzenmacher, J. Ducrée, R. Zengerle, F. Von Stetten, Energy harvesting by implantable abiotically catalyzed glucose fuel cells, J. Power Sources, 182 (2008) 1-17.
[92] C. Corti, R. Holliday, D. Thompson, Progress towards the commercial application of gold catalysts, Top. Catal., 44 (2007) 331-343.
[93] M.C. Leopold, E.F. Bowden, Influence of Gold Substrate Topography on the Voltammetry of Cytochrome c Adsorbed on Carboxylic Acid Terminated Self-Assembled Monolayers, Langmuir, 18 (2002) 2239-2245.
[94] M. Falk, Z. Blum, S. Shleev, Direct electron transfer based enzymatic fuel cells, Electrochim. Acta, 82 (2012) 191-202.
[95] R.A.S. Luz, A.R. Pereira, J.C.P. de Souza, F.C.P.F. Sales, F.N. Crespilho, Enzyme Biofuel Cells: Thermodynamics, Kinetics and Challenges in Applicability, ChemElectroChem, 1 (2014) 1751-1777.
[96] M. Cooney, V. Svoboda, C. Lau, G. Martin, S. Minteer, Enzyme catalysed biofuel cells, Energy Environ. Sci., 1 (2008) 320-337.
[97] T. Sakurai, K. Kataoka, Basic and applied features of multicopper oxidases, CueO, bilirubin oxidase, and laccase, Chem. Rec., 7 (2007) 220-229.
[98] S. Boland, D. Leech, A glucose/oxygen enzymatic fuel cell based on redox polymer and enzyme immobilisation at highly-ordered macroporous gold electrodes, Analyst, 137 (2012) 113-117.
[99] U. Salaj-Kosla, S. Pöller, W. Schuhmann, S. Shleev, E. Magner, Direct electron transfer of *Trametes hirsuta* laccase adsorbed at unmodified nanoporous gold electrodes, Bioelectrochemistry, 91 (2013) 15-20.
[100] L. Deng, F. Wang, H. Chen, L. Shang, L. Wang, T. Wang, S. Dong, A biofuel cell with enhanced performance by multilayer biocatalyst immobilized on highly ordered macroporous electrode, Biosens. Bioelectron., 24 (2008) 329-333.
[101] M. Tominaga, M. Ohtani, I. Taniguchi, Gold single-crystal electrode surface modified with self-assembled monolayers for electron tunneling with bilirubin oxidase, Phys. Chem. Chem. Phys., 10 (2008) 6928-6934.
[102] K. Murata, K. Kajiya, N. Nakamura, H. Ohno, Direct electrochemistry of bilirubin oxidase on three-dimensional gold nanoparticle electrodes and its application in a biofuel cell, Energy Environ. Sci., 2 (2009) 1280-1285.
[103] M. Falk, V. Andoralov, Z. Blum, J. Sotres, D.B. Suyatin, T. Ruzgas, T. Arnebrant, S. Shleev, Biofuel cell as a power source for electronic contact lenses, Biosens. Bioelectron., 37 (2012) 38-45.

Figure captions

Figure 1. Main view (A) and side view (B) scanning electron microscope (SEM) images of NPG leaf (reprinted with permission from [69]). (C) Transmission electron microscope (TEM) image of NPG (reprinted with permission from [70]). (D) Contact mode atomic force microscope (AFM) images of NPG. Scan area: 500×500 nm^2. (E) Height profile of a cross section along the line as indicated by a and b in (D) (reprinted with permission from [69]). (F) TEM image of a [01] nanopore and the corresponding diffraction pattern (inset). (G) High-angle annular dark-field-scanning TEM (HAADF-STEM) image of the labeled square indicated as b in (F). The intensity profile (inset) along the dotted line represents a stepped surface. (H) HAADF-STEM image of the labeled square indicated as d in (F) (reprinted with permission from [51]).

Figure 2. Cyclic voltammogram for a dealloyed NPG electrode in 1 M H_2SO_4 (scan rate: 0.1 V s^{-1}).

Figure 3. (A) Bright-field TEM image of NPG/MnO_2 hybrid materials for electrochemical supercapacitors (reprinted with permission from [35]). (B) HRTEM image of the NPG/MnO_2 hybrid showing nanocrystalline MnO_2 with a grain size of ~5 nm. (C) HAADF-STEM image taken from a gold/MnO_2 interface region. (D) HRTEM image of the NPG/amorphous tungsten sulfide for electrochemical hydrogen evolution (reprinted with permission from [34]). (E) TEM image of NPG decorated with a thin glucose oxidase doped silica film generated by electro-assisted sol-gel process (unpublished results). The enzyme was catalytically active. (F) TEM image of NPG/poly(3,4-ethylenedioxythiophene) biocomposite with glucose oxidase entrapped in the film (reprinted with permission from [33]).

Figure 4. (A) Schematic diagram of the porosity evolution process during dealloying of a Ag/Au alloy (modified from [6]). (B) 12-carat Ag/Au (white gold) leaf. (C) NPG leaf attached onto a GCE with a diameter of 4 mm. (D) Diagram of the layered Ag/Au alloy film obtained by magnetron sputtering (not to scale), modified from [27]. (E) Schematic diagram of NPG fabrication using in-situ electrodeposition and dealloying, modified from [28].

Figure 5. Schematic diagram of hard template route (A), dynamic hydrogen bubble template method (B) and anodization of gold electrodes (C). SEM images of assembly of five layers of 680 nm silica nanoparticles on electrode (D) and the final macroporous gold structure obtained (E) (reprinted with permission from [40]). The SEM images of porous Au via dynamic hydrogen bubble template method (F) (Copyright 2015, reprinted from [44]) and anodization (G) (reprinted with permission from [45]).

Figure 6. Methods of immobilising enzyme on NPG, including physical adsorption of lipase (A)

(reprinted with permission from [38]), covalent bonding in the assistance of SAM (B) (reprinted with permission from [69]) and entrapment within conducting polymers (C) (reprinted with permission from [33]).

Figure 7. Schematic diagram of a NPG based glucose/O_2 BFC fabricated by drop-casting a solution of osmium redox polymer, enzyme and cross-liners. Reproduced from [75] with permission from The Royal Society of Chemistry.

Figure 8. Schematic diagram of a cross-section of NPG electrodes with adsorbed *Mv*BOD without (A) and with P017-epoxy caps (C) and their electrochemical behaviors (B, D) towards Ar (dotted line) and O_2 (full and dashed line for the first and second scan), respectively. Inset of (B): SEM image of the surface of a NPG electrode. Inset of (D): the proposed structure of P017-epoxy. Conditions: 0.1 M pH 7.0 citrate-phosphate buffer, scan rate of 5 mV s^{-1}. Reproduced from [76] with permission.

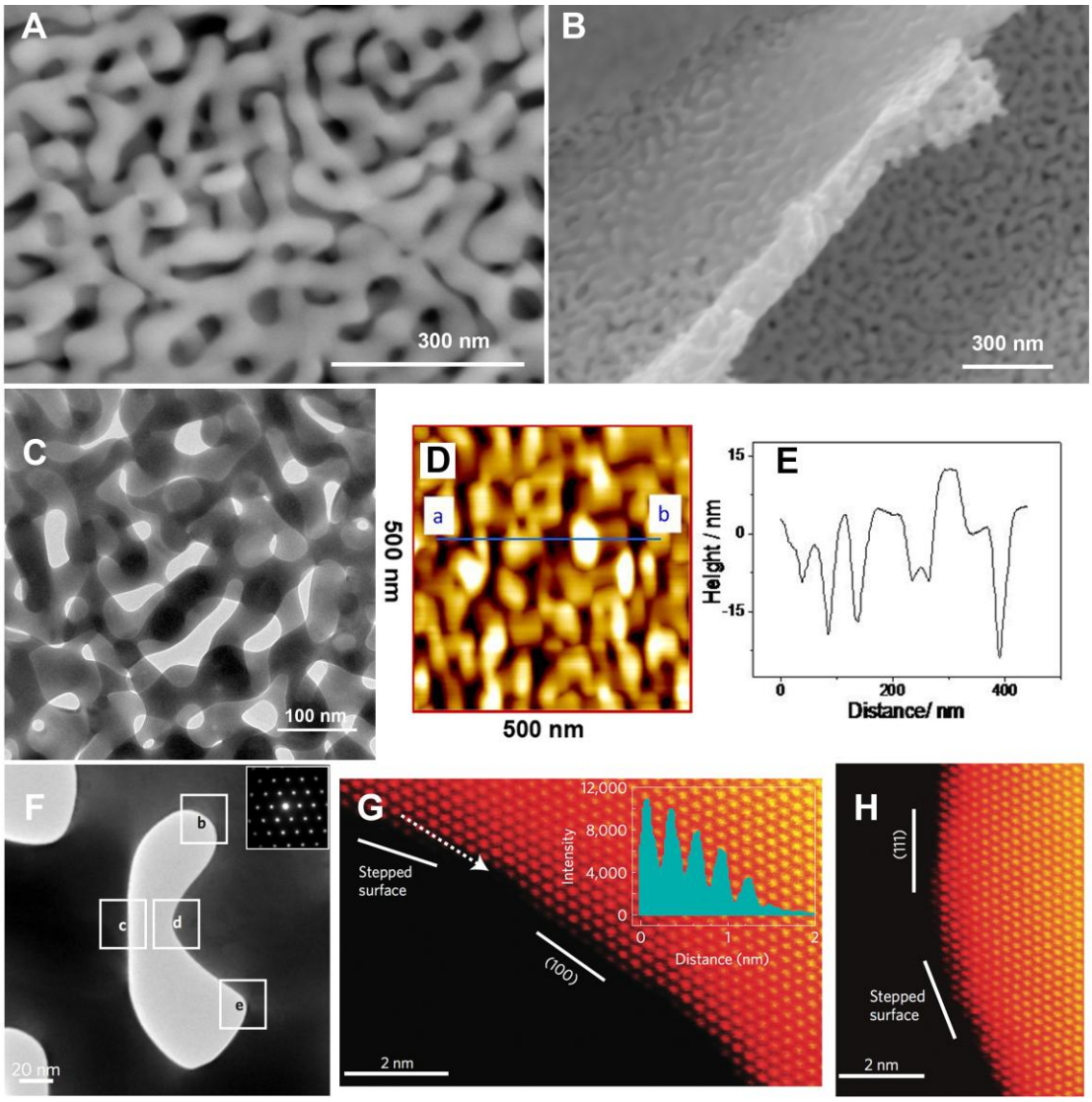
A
300 nm
B
300 nm
C
100 nm
D
a
b
500 nm
500 nm
E
15
0
-15
Height / nm
0
200
400
Distance/ nm
F
b
c
d
e
20 nm
G
Stepped
surface
12,000
8,000
4,000
0
Intensity
0
1
2
Distance (nm)
(100)
2 nm
H
(111)
Stepped
surface
2 nm

Fig. 1

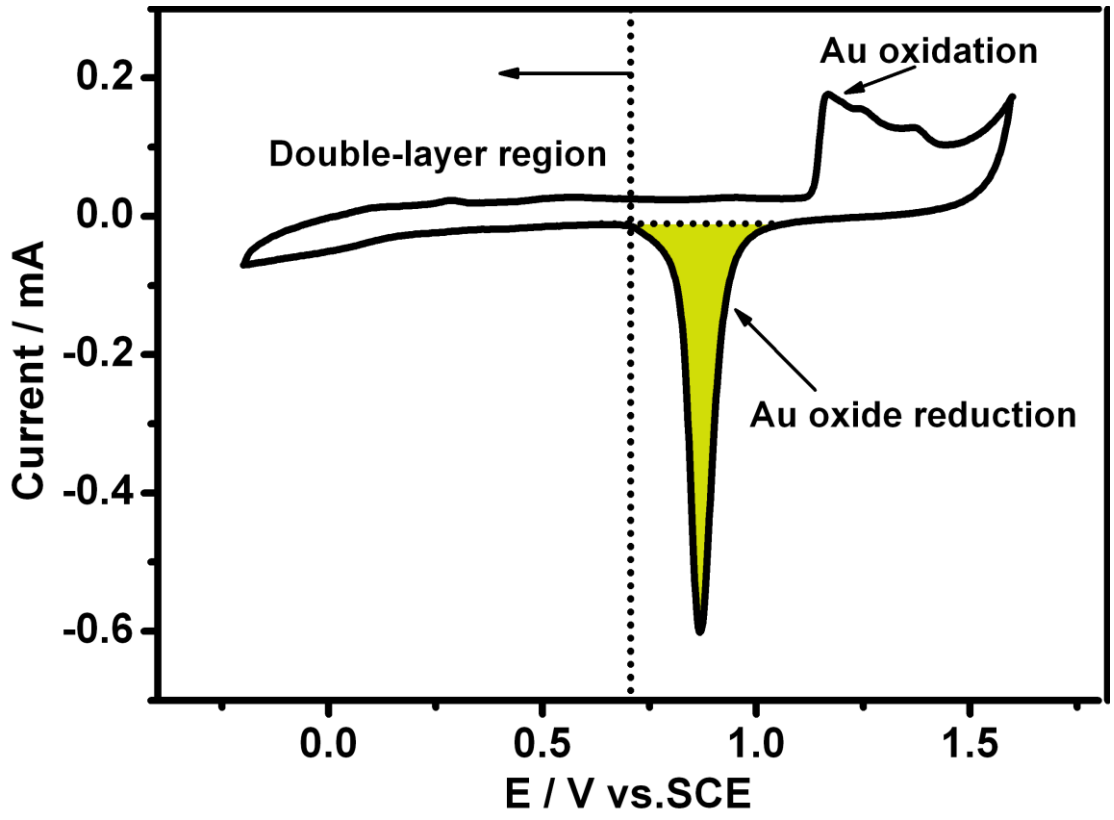
Au oxidation
Double-layer region
Au oxide reduction
Current / mA
0.2
0.0
-0.2
-0.4
-0.6
0.0
0.5
1.0
1.5
E / V vs.SCE

Fig. 2

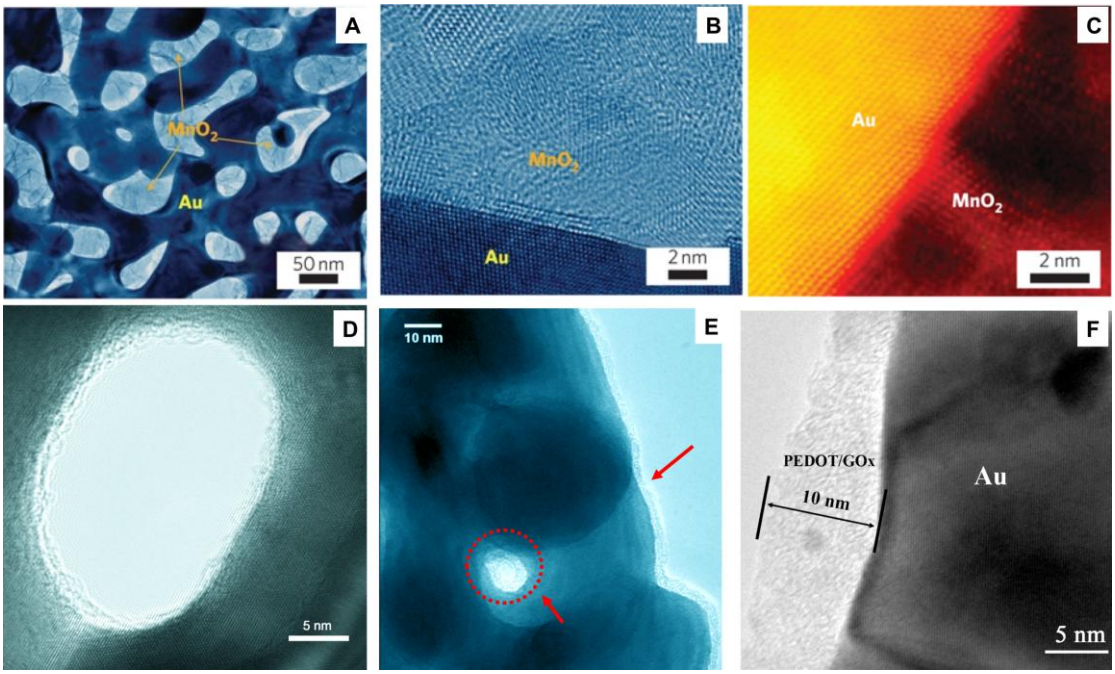
A
MnO2
Au
50 nm
B
MnO2
Au
2 nm
C
Au
MnO2
2 nm
D
5 nm
E
10 nm
F
PEDOT/GOx
10 nm
Au
5 nm

Fig. 3

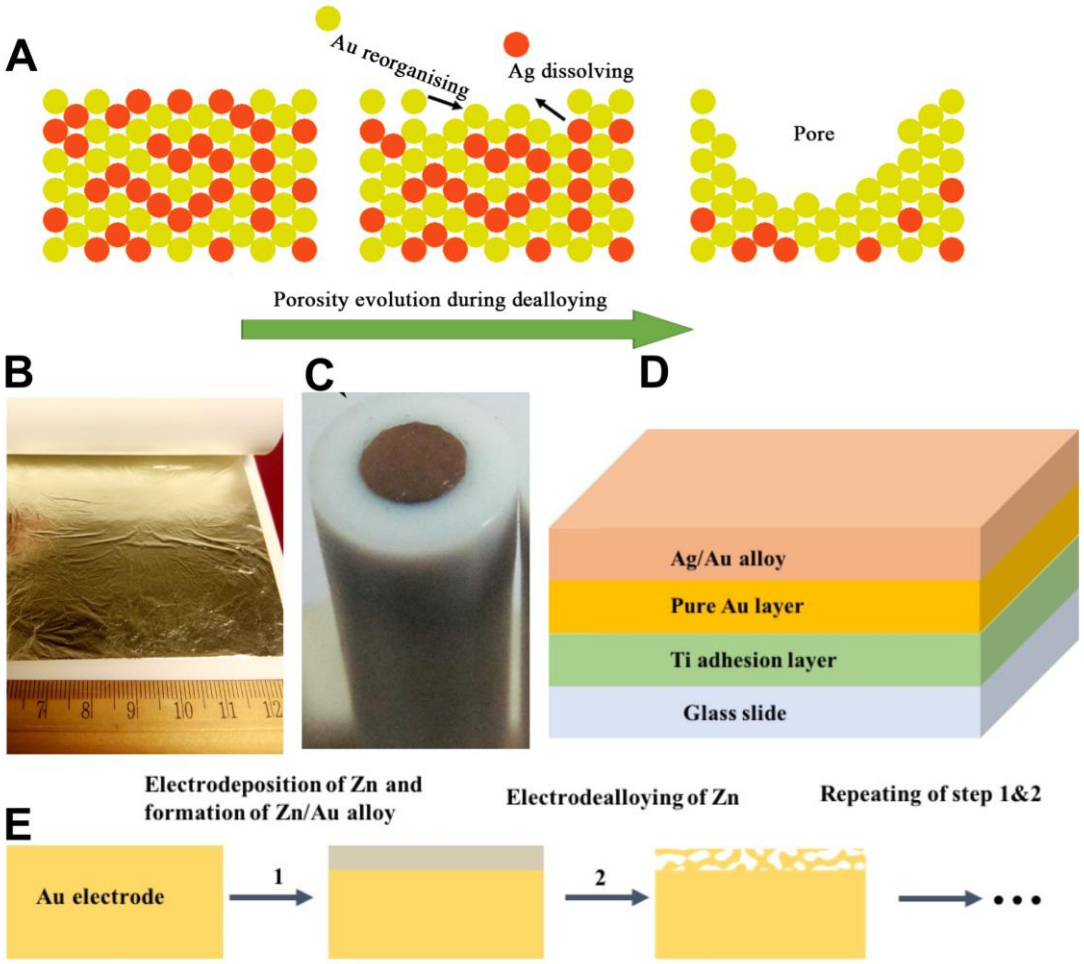
A
Au reorganising
Ag dissolving
Pore
Porosity evolution during dealloying
B
C
D
Ag/Au alloy
Pure Au layer
Ti adhesion layer
Glass slide
Electrodeposition of Zn and formation of Zn/Au alloy
Electrodealloying of Zn
Repeating of step 1&2
E
Au electrode
1
2

Fig. 4

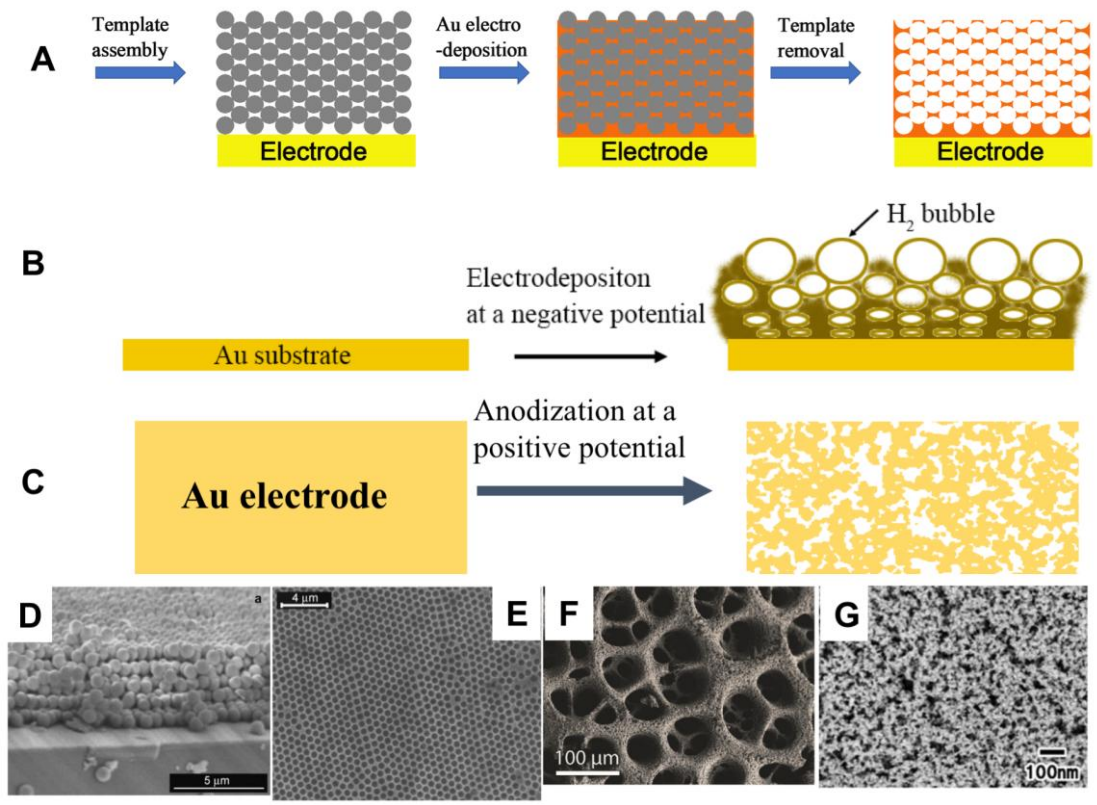
A
Template assembly
Electrode
Au electro -deposition
Electrode
Template removal
Electrode
B
H2 bubble
Electrodepositon at a negative potential
Au substrate
C
Au electrode
Anodization at a positive potential
D
a
5 μm
4 μm
E
F
100 μm
G
100nm

Fig. 5

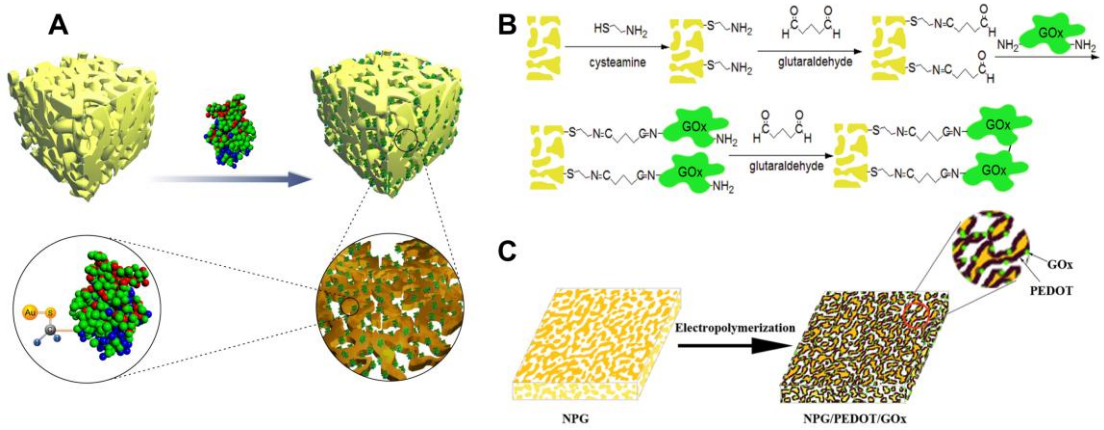
A
B
cysteamine
glutaraldehyde
GOx
glutaraldehyde
C
Electropolymerization
GOx
PEDOT
NPG
NPG/PEDOT/GOx

Fig. 6

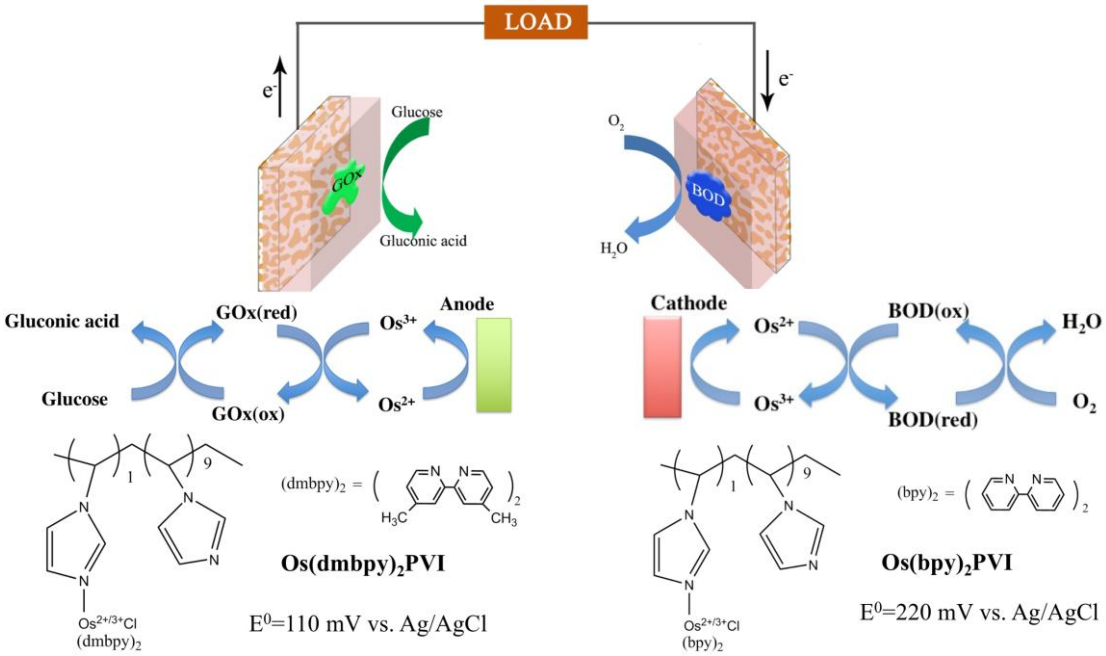
LOAD
e-
e-
Glucose
Gluconic acid
GOx
O2
H2O
BOD
Gluconic acid
Glucose
GOx(red)
GOx(ox)
Os3+
Os2+
Anode
Cathode
Os2+
Os3+
BOD(ox)
BOD(red)
H2O
O2
(dmbpy)2 =
H3C
CH3
Os(dmbpy)2PVI
E0=110 mV vs. Ag/AgCl
Os2+/3+Cl
(dmbpy)2
(bpy)2 =
Os(bpy)2PVI
E0=220 mV vs. Ag/AgCl
Os2+/3+Cl
(bpy)2

Fig. 7

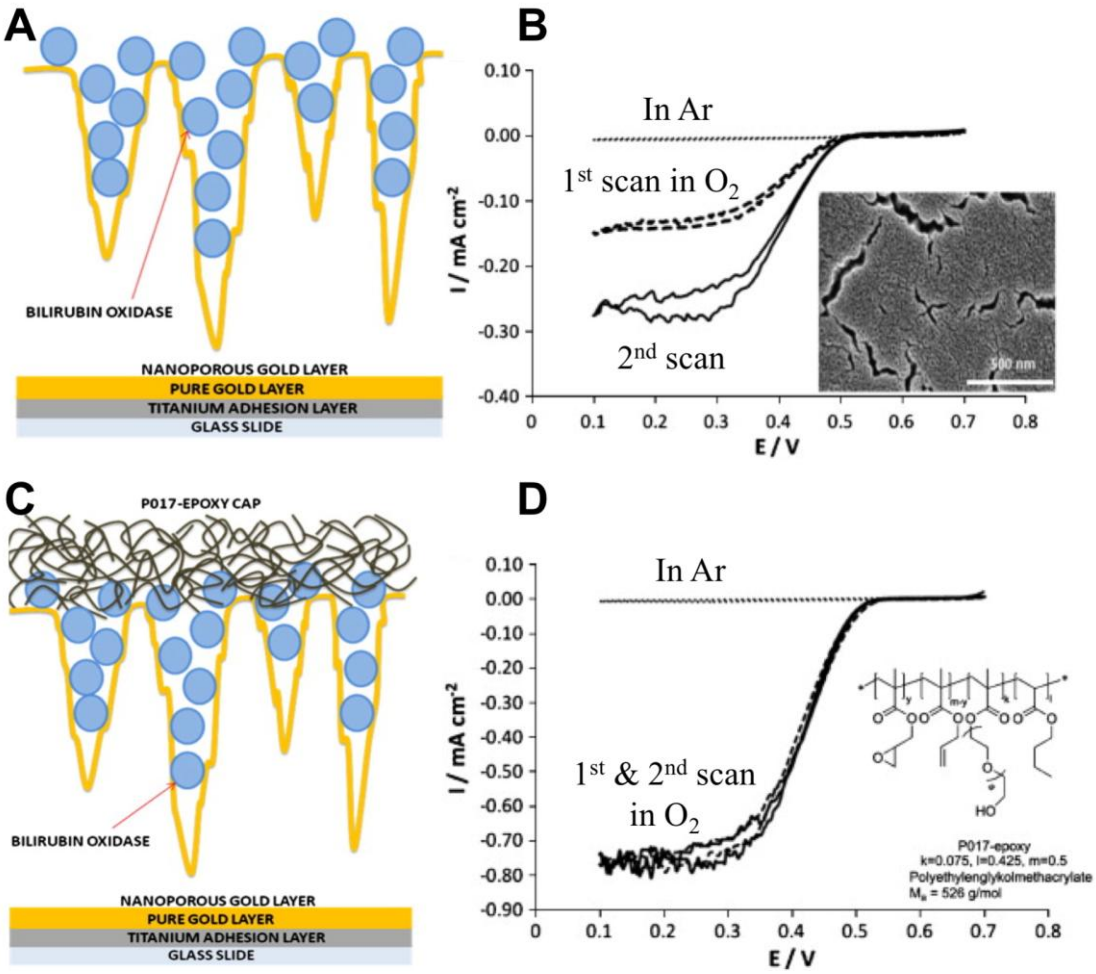
A
BILIRUBIN OXIDASE
NANOPOROUS GOLD LAYER
PURE GOLD LAYER
TITANIUM ADHESION LAYER
GLASS SLIDE
B
In Ar
1st scan in O2
2nd scan
500 nm
I / mA cm-2
E / V
C
P017-EPOXY CAP
BILIRUBIN OXIDASE
NANOPOROUS GOLD LAYER
PURE GOLD LAYER
TITANIUM ADHESION LAYER
GLASS SLIDE
D
In Ar
1st & 2nd scan
in O2
P017-epoxy
k=0.075, l=0.425, m=0.5
Polyethylenglykolmethacrylate
Mn = 526 g/mol
I / mA cm-2
E / V

Fig. 8

Table 1. Comparison of porous gold materials fabricated with different methods.

Method	Substrate	Morphology	Pore size
Dealloying	Au or Si, glass etc.	Bicontinuous pores and ligaments; Randomly distributed and interconnected pores	~5-700 nm
Hard template route	Au or Pt	Periodically arranged pores; Interconnected pores	100-2000 nm
Dynamic hydrogen bubble template method	Au or Pt	Open structure with larger pores on the top of smaller ones; Interconnected pores	~1-30 μm
Anodization	Au	Spongelike configuration	~20 nm

Highlights

- The fabrication and characterization of dealloyed NPG has been briefly summarized.
- The properties of NPG for bioelectrochemistry have been described in detail.
- The applications of dealloyed NPG in biosensors and biofuel cells have been reviewed.